Surface Ru enriched structurally ordered intermetallic PtFe@PtRuFe core-shell nanostructure boosts methanol oxidation reaction catalysis

Qingmei Wang, Siguo Chen*, Pan Li, Shumaila Ibraheem, Jia Li, Jianghai Deng, Zidong Wei*

The State Key Laboratory of Power Transmission Equipment & System Security and New Technology, Chongqing Key Laboratory of Chemical Process for Clean Energy and Resource Utilization, School of Chemistry and Chemical Engineering, Chongqing University, Chongqing 400044, China

A B S T R A C T

Atomic-level control of the surface composition and atomic arrangement of multimetalic alloy nanocatalyst has emerged as an effective strategy to optimize their catalytic performance. By integrating the space-confined alloying and surface engineering strategies, we demonstrate a new class of core-shell structured PtFe@PtRuFe nanocatalyst, composed of an ordered PtFe intermetallic core with a 3–5 atomic-layers-thick PtRuFe shell. The well-defined PtFe@PtRuFe core-shell nanostructure exhibits excellent anti-CO poisoning ability and resistance to Fe leaching, achieving a factor of 1.68 enhancement in mass activity and a factor of 1.57 improvement in specific activity toward methanol oxidation reaction (MOR) compared to the state-of-the-art PtRu/C catalysts. Furthermore, the CO anodic oxidation on the PtFe@PtRuFe catalyst surface (0.39 V) starts much earlier than on the commercial PtRu/C (0.43 V) and Pt/C (0.83 V) catalysts. The enhanced MOR activity and anti-CO poisoning ability of the PtFe@PtRuFe catalyst is mainly attributed to the well-defined core-shell structure and favorable composition as well as the charge transfer from Fe/Ru to Pt and thusly be weakened Pt-CO_{ads} adsorption energy. This novel core-shell structured nanocatalyst provide a new direction to reduce the usage of noble metal, tune the surface composition and atomic arrangement, enhance the activity and stability of multimetalic alloy nanocatalyst.

1. Introduction

The exploitation of anodic catalysts with excellent catalytic performance in direct methanol fuel cells (DMFCs) has been ongoing several decades [1–5]. PtRu bimetallic nanomaterials have been recognized as the best-performing anti-CO poisoning electrocatalysts for the methanol oxidation reaction (MOR) to date, and this can be explained by the Watanabe-Motoo bifunctional mechanism [6,7]. The oxophilic metal, Ru, modified to Pt can provide adsorbed hydroxyl groups (OH_{ads}) at lower potential than on pristine Pt, which serves as the oxidant to remove the adsorbed carbon monoxide (CO_{ads}) on Pt by oxidizing it to CO_2 [8,9]. However, in PtRu system, the oxidation potential of CO_{ads} on Pt sites (larger than 0.35 V vs RHE) [10,11] is still more positive than the formation potential of OH_{ads} on adjacent Ru sites (0.2~0.3 V vs RHE) [12], which makes the removal of CO_{ads} on Pt is always the rate-determining step and requires further to tune the electronic structure of Pt. This fact, in combination with the high cost of Pt and Ru, has fueled the search for inexpensive MOR electrocatalysts with improved catalytic performance [13,14].

One promising way to boost the MOR activity of PtRu bimetallic alloy is to construct ternary PtRuM alloys (M = Fe [15], Co [13], Ni [17], Pd [16], etc.,) that have enhanced activity but use less Pt and Ru. However, previous studies have mainly focused on the disordered PtRuM alloys, which have varying surface composition and thus randomly distributed active sites [17–19]. Such disordered structure typically suffer from insufficient stability because of the less noble metal is continuously leaching during electrochemical cycling under acidic conditions [20–22]. From the structural perspective, the ordered intermetallic phases, with definite composition and atomic arrangement, can give the predictable control over geometric and electronic effects for catalysis design and optimization, which can achieve both high activity and stability in practical DMFCs applications [23]. Nevertheless, the synthesis of small-sized ordered PtRuM trimetallic alloy nanoparticles (NPs) has never been reported thus far. This is due to the fact that the formation of ordered PtRuM trimetallic alloy structure requires the preferential synthesis of well-defined disordered PtRuM alloys via conventional wet-chemical methods, which contains tedious multistep reactions and rigorous experimental conditions and purification processes [24–28]. Besides, high-temperature annealing is generally needed to transfer the pre-synthesized disordered PtRuM
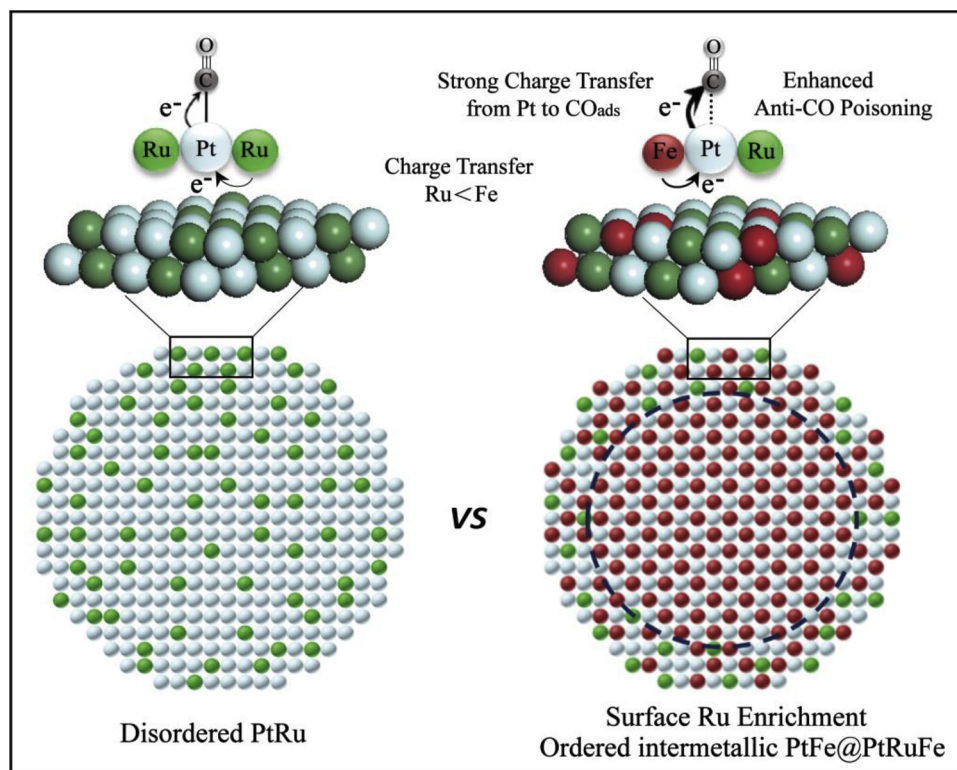
Fig. 1. The demonstration of disordered PtRu catalyst and the surface Ru enrichment structurally ordered intermetallic PtFe@PtRuFe core-shell nanostructure and the corresponding illustration of the electron transfer when CO adsorbed on the PtRu and PtRuFe surface. The charge transfer on the PtRuFe surface is stronger than in the PtRu surface. The bonding (dashed lines) of Pt–CO in PtRuFe surface is weaker than the disordered PtRu surface (solid lines).

alloy into ordered PtRuM alloy, which may lead to NPs sintering and difficulty in controlling the surface composition and atomic arrangement of NPs [29]. Therefore, the exploration of a simple and cost-efficient alloying methodology where particle size, composition, and atomic arrangement can be precisely controlled is imperative, but, remains an open challenge.

By integrating the space-confined alloying and surface engineering strategies, we designed a PtFe@PtRuFe core-shell nanostructure (Fig. 1), composed of an ordered PtFe intermetallic core covered with a 3–5 atomic-layer-thick PtRuFe shell. The overall concept is shown in Figure. S1. The starting material is a well-constructed dual-shell Pt/C@PDA-Ru^{3+}/Fe^{3+}@SiO$_2$ composite in which the Pt/C core is covered with an inner polydopamine (PDA) shell and an outer silica (SiO$_2$) shell. The inner PDA shell was used as the precursor of nitrogen-doped carbon (NC) shell and a strong chelating agent to homogeneously adsorb Ru^{3+} and Fe^{3+}, while the outer SiO$_2$ layer was used to create an encapsulated space to prevent NPs sintering during high-temperature annealing. The high-temperature, in junction with the H_2/N_2 reduction atmosphere, drives the "reduction" and "diffusion" of absorbed Fe^{3+} with smaller atomic radius (1.27 Å) and relatively higher diffusion rate into the interior of Pt to form ordered intermetallic PtFe core, while the reduced Ru atoms with larger atomic radius (1.32 Å) and smaller diffusion rate enrich at the surface to form PtRuFe shell. For the ordered intermetallic PtFe core, recent studies indicate that the ordered phases with high enthalpy showed significantly less leaching of their non-noble metal components than their alloy counterparts with identical composition when electrochemically cycled in acidic solutions [30–38]. Moreover, the incorporation of Fe into PtRu shell can transfer more electrons to Pt than only PtRu, which will further weaken the Pt-CO$_{ads}$ adsorption energy and facilitate the removal of CO$_{ads}$ on Pt sites [39,40]. Benefiting from this unique surface composition and atomic arrangement, the core-shell PtFe@PtRuFe NPs exhibit excellent MOR activity and enhanced durability than the state-of-the-art PtRu/C catalysts, making them a promising candidate for the next generation DMFCs. Most importantly, our work gives an illustration of a simple and cost-efficient alloying methodology for precisely adjusting the surface composition

and atomic arrangement which indeed provides guidance for future fabrication of catalytic materials in the field of green chemistry energy conversion.

2. Experimental

2.1. Chemicals and materials

Commercial Pt/C catalyst (JM, 20 wt. % Pt, Pt particle size: 2–5 nm). 4-(2-ethylamino) benzene-1,2-diol ($C_8H_{11}O_2N$, 90%). Ferric chloride (FeCl$_3$, 99%), Antimony trichloride (RuCl$_3$,99%), Tetraethyl orthosilicate (Si(OC$_2$H$_5$)$_4$ 98%), Tris(hydroxymethyl)aminomethane ($C_4H_{11}NO_3$, 99.5%), above of the material and the nafion (5% in a mixture of lower aliphatic alcohols and water) were all purchased from adamas.

2.2. Synthesis of core shell structured PtFe@PtRuFe catalyst

50 mg commercial Pt/C catalyst (JM, 20 wt. % Pt) was dispersed in the solution mixtures of deionized water (30 mL) and ethanol (30 mL). The mixture was then stirred ultrasonically at room temperature for 10 h to achieve homogeneous dispersion, and then 20 mg dopamine dissolved in 20 mL Tris-HCl (50 mM, pH ≈ 8.5) solution was added. The mixture was stirred for 12 h at room temperature. The obtained core-shell structured nanocomposite (Pt/C@PDA) was collected by centrifugation and washed with deionized water and then dried at 60°C for 12 h. The obtained Pt/C@PDA was stirred with FeCl$_3$ and RuCl$_3$ in deionized water to form Pt/C@PDA-$Ru^{3+}$$Fe^{3+}$ suspension. After 12 h stirring, solution of 2 mL tetraethoxysilane (TEOS) and 2 mL HCl (pH = 3) were added to the Pt/C@PDA-$Ru^{3+}$$Fe^{3+}$ suspension and the mixture was mixed at room temperature for 2 h to get a homogeneous mixture. The homogeneous mixture was moved to glass petri dishes and allowed to slowly evaporate in empty environments until the composite films (Pt/C@PDA-$Ru^{3+}$$Fe^{3+}$@SiO$_2$) formed. For pyrolysis of the Pt/C@PDA-$Ru^{3+}$$Fe^{3+}$@SiO$_2$, the solid films were heated at a rate of 5 °C / min to 800°C and maintained for 4 h under flowing 10%H_2/90%Ar to

obtain pyrolyzed PtFe@PtRuFe@SiO$_2$ composites. After slowly cooling the sample to room temperature, the PtFe@PtRuFe@SiO$_2$ composites were etched by HF to removal the silica layers and excess Fe species. The resulting products were washed with anhydrous alcohol and deionized water and finally dried under vacuum at 60 °C for 24 h.

2.3. Characterization

Transmission electron microscopy (TEM) was carried out on a Zeiss LIBRA 200 FETEM instrument operating at 200 kV. High-angle annular dark-field scanning transmission electron microscope (HAADF-STEM)-energy-dispersive X-ray spectroscopy (EDS) were taken on a JEM-ARM200 F transmission electron microscope operated at 300 kV. X-ray Photoelectron Spectroscopy (XPS) analysis was conducted on a PE PHI-5400 spectrometer equipped with a monochromatic Al X-ray source (Al KR, 1.4866 keV). X-ray diffraction data were collected on an XRD-6000 using Cu KR radiation at a step rate of 2° min^{-1}. The concentration of catalysts was determined by the inductively coupled plasma mass spectrometry (Thermo Fisher Scientific, iCAP6300 ICP-MS).

2.4. Electrochemical measurements

All electrochemical experiments were performed in a standard three-electrode cell at room temperature. The cell consisted of a glassy carbon working electrode (GC electrode, 5 mm in diameter, PINE: AFE3T050GC), an Ag/AgCl (3 M KCl) reference electrode, and a platinum wire counter electrode. All potentials in this study, however, are given relative to the reversible hydrogen electrode (RHE). Catalyst Deposition on the Working Electrode.[1] The working electrodes were prepared by applying catalyst ink onto glassy carbon (GC) disk electrodes. In brief, the electrocatalyst was dispersed in ethanol and ultra-sonicated for 30 min to form a uniform catalyst ink (0.5 mg mL^{-1}). A total of 5 μL of well-dispersed catalyst ink was applied onto a pre-polished GC disk. After drying at room temperature, a drop of 0.05 wt% Nafion solution was applied onto the surface of the catalyst layer to form a thin protective film. The prepared electrodes were dried at room temperature before electrochemical tests. Before electrochemical measurements, all the electrodes were pretreated by cyclic voltammetry (CV) at potential between 0.05 V to 1.2 V at a sweep rate of 50 mv/s for 50–100 cycles to remove any surface contamination in 0.1 M HClO$_4$. The methanol oxidation reaction (MOR) was conducted in N$_2$-saturated 0.1 M HClO$_4$ solution containing 0.5 M methanol. The CO Stripping measurements were conducted in N$_2$-saturated 0.1 M HClO$_4$ solution which was purged with CO before the measurement. The scan rate for measurement was 10 mV/s. Chronoamperometry was carried out at the constant potential of 0.75 V in 0.1 M HClO$_4$ solution containing 0.5 M methanol. The electrochemical surface area (ECSA) of Pt in the catalysts using the following equation:

$$ECSA = \frac{Qco}{0.42 \times [Pt]}$$

where Qco is the charge due to the integrated area of the CO dissolved peak, 0.42 mC cm^{-2} is the electrical charge associated with monolayer adsorption of hydrogen on Pt, and [Pt] is the loading of Pt on the working electrode.

3. Results and discussion

The crystal structure of the as-prepared PtFe@PtRuFe sample was first investigated by powder X-ray diffraction (XRD). As shown in Fig. 2a, the characteristic peaks of PtFe@PtRuFe slightly shift to higher angles as compared with Pt/C, indicating that Fe^{3+} and Ru^{3+} have been successfully reduced and incorporated into Pt to form alloy with a concomitant lattice contraction. Moreover, the PtFe@PtRuFe sample exhibits a set of additional sharp super lattice peaks at 2θ of 32.85 for (110), 53.61 for (201), 60.30 for (112), 70.42 for (202), 74.12 for

(221), 78.50 for (130), and 86.4 for (113), indicating the formation of ordered intermetallic face-centered tetragonal (fct) PtFe alloy (PDF:43-1359) [41–43]. The morphology, structure and composition profiles of the PtFe@PtRuFe NPs were further characterized by transmission electron microscopy (TEM) and atomically resolved aberration-corrected high-angle annular dark-field–scanning transmission electron microscopy (HAADF-STEM) in combination with energy-dispersive X-ray spectroscopy (EDX). As shown in Fig. 2b and Figure. S2, the obtained PtFe@PtRuFe NPs are homogeneously dispersed on carbon support with small particle size diameter of 4–5 nm, indicating that the sintering of NPs during high-temperature annealing can be effectively prevented by encapsulating the NPs in a removable silica protecting space. For comparison, the TEM images and the corresponding particle size statistics Pt/C and PtRu/C catalysts after high temperature treatment without SiO$_2$ protecting shell are also shown in Figure. S3.

High resolution TEM (HRTEM) image reveals that the smooth surface of carbon is covered with a thin layer of NC shell (Figure. S4). The average thickness of the NC shells was ~2 nm. Figure. S5 also confirming that the space-confined SiO$_2$ outer layer is successfully removed by low concentration hydrofluoric acid. The HAADF-STEM images (Fig. 2c and Figure. S6) and the corresponding fast Fourier transform (FFT) of selected core area analysis (insert in Fig. 2c) further confirm the ordered intermetallic alloy structure, and the unit cell projected along the [-110] axis exhibits a periodic line array of Fe columns stacked by Pt columns. The EDX elemental mapping images (Fig. 2d-i) show that elements of Pt, Ru and Fe exhibit a similar size as that in the STEM image, further confirming that the absorbed Ru^{3+} and Fe^{3+} ions have been successfully reduced and diffused into Pt to form PtFe@PtRuFe NPs. Particularly, most of the Ru atoms are located at the edges of NP, while the Fe atoms incline to scattered into the center. This result is consistent with the electron energy loss spectroscopy (EELS) line scan profiles of Pt, Ru, Fe elements (Fig. 2g) and the corresponding Ru/Pt and Fe/Pt atomic ratios. As shown in Figure. S7, the Ru/Pt ratio (~0.3) in the external of NP is larger than in the interior (~0.1) whereas opposite of the Fe/Pt ratios. The absorbed Fe^{3+} with smaller atomic radius and relatively higher diffusion rate into the interior of Pt to form ordered intermetallic PtFe core, while the Ru^{3+} with larger atomic radius and smaller diffusion rate enrich at the surface to form PtRuFe shell. Further detailed analysis of selected NP shows that the core of ordered PtFe phase is covered with a 3–5 layer of disordered PtRuFe shell (Figure. S8).

The elemental compositions and chemical status of PtFe@PtRuFe sample were further investigated by X-ray photoelectron spectroscopy (XPS) measurement. The presence of Pt, Ru, Fe, N, C, and O was confirmed in the XPS survey of PtFe@PtRuFe sample (Fig. 3a). The N1s spectra can be deconvoluted into three peaks, attributed to the pyridinic-N (398.21 eV), pyrrolic-N (400.54 eV) and quaternary-N (401.20 eV), respectively (Fig. 3b), indicating that PDA precursor has been successfully transformed into NC shell. The Pt4f spectra of PtFe@PtRuFe show two peaks that can be assigned to Pt 4f$_{7/2}$ and Pt 4f$_{5/2}$, and can be further split into two doublets, associated with the metallic Pt and Pt oxides (Fig. 3c). The peak at 280.6 eV represents the metallic Ru, and the peaks at 281.3 and 281.8 eV indicate the Ru oxides (Fig. 3d). Similarly, the Fe 2p can be split into three doublets, associated with metallic Fe and Fe oxides (Fig. 3e). It is obvious that the high content of metallic state on catalyst would provide more effective active sites for MOR [44]. Furthermore, a larger negative shift in Pt 4f$_{7/2}$ binding energy is observed for PtFe@PtRuFe (0.48 eV) than PtRu/C catalyst (0.25 eV) when compared with pristine Pt/C (Fig. 3f), indicating that more electrons have been transferred to Pt in PtFe@PtRuFe sample than in PtRu/C due to the larger electronegativity of Fe than Ru (Pt: 2.28, Ru: 2.20, Fe: 1.80) [45]. The larger downshift in Pt4f binding energy will weaken the Pt-CO$_{ads}$ adsorption energy and thus facilitate the removal of CO$_{ads}$ and promote the C−H cleavage on Pt sites [46,47].

Since adsorbed CO is the main intermediate formed during MOR in DMFCs, the anti-CO poisoning ability of the PtFe@PtRuFe catalysts is
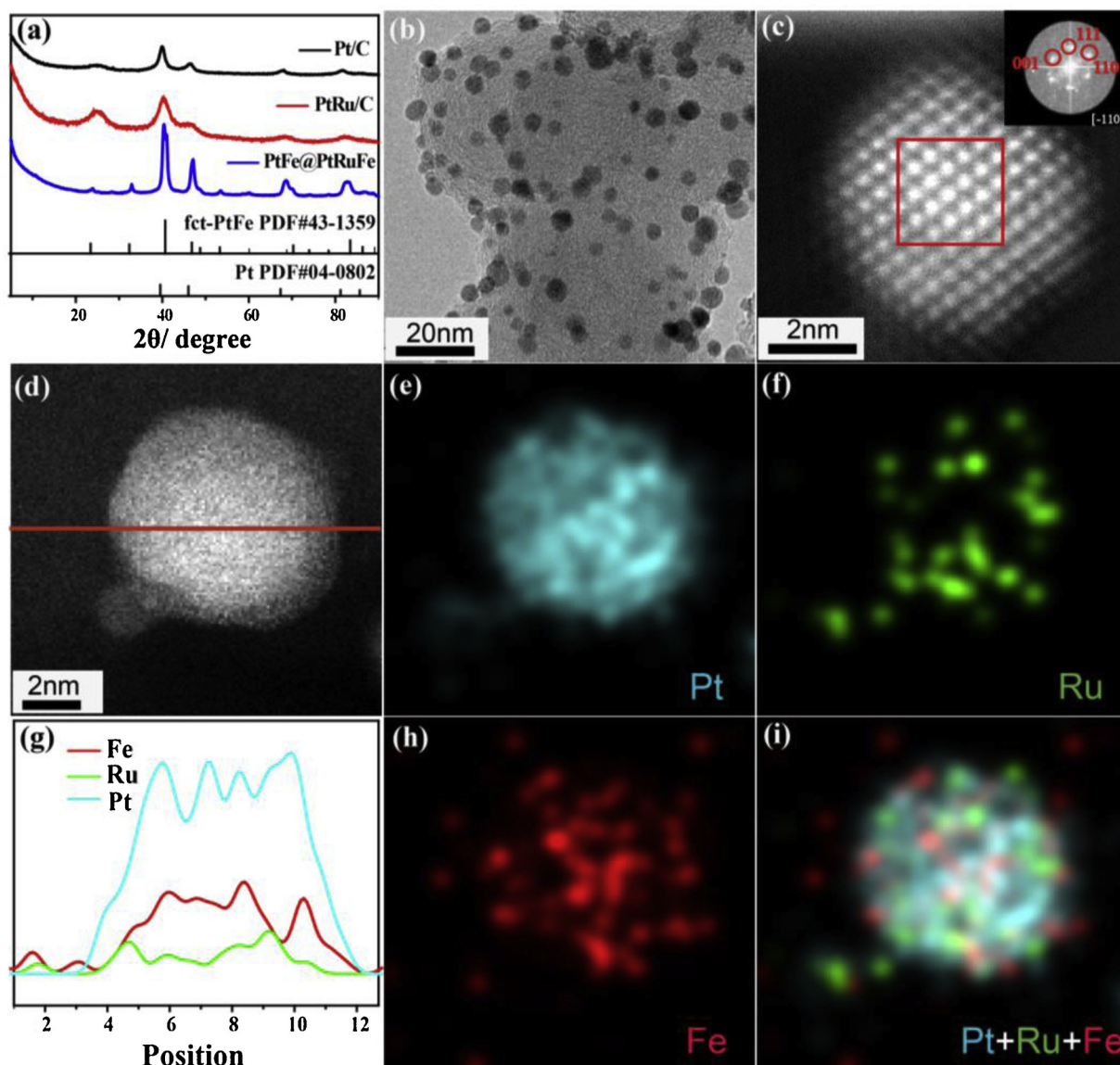
Fig. 2. (a) XRD patterns of Pt/C, PtRu/C and PtFe@PtRuFe catalysts. (b) TEM and (c) HRTEM images of PtFe@PtRuFe NP and its corresponding FFT image. (d) HAADF-STEM image of a typical PtFe@PtRuFe NP and the corresponding EDX line-scanning profile(g), and elemental mapping images of Pt (e), Ru (f), Fe (h), and the overlap of three elements (i).

extremely significant. Fig. 4a compares the CO stripping voltammograms of PtFe@PtRuFe, PtRu/C and Pt/C catalysts. The onset potential for CO oxidation on PtFe@PtRuFe catalyst (0.39 V) starts much earlier than on the commercial PtRu/C (0.43 V) and Pt/C (0.83 V) catalysts, illustrating that the pre-adsorbed CO on PtFe@PtRuFe catalyst is easier to be oxidized than on the PtRu/C and Pt/C catalysts. The electrochemical surface area (ECSA) was calculated from the CO oxidation charge after subtracting the background current. The specific value of ECSA based on the Pt mass for the PtFe@PtRuFe was estimated to be 53 $m^2 g^{-1}$ (Fig. 4b), which is slightly higher than the commercial PtRu/C (49 $m^2 g^{-1}$) catalyst, suggesting that more Pt active sites in PtFe@PtRuFe were exposed for MOR [48,49].

Fig. 4c compares the MOR performance of the PtFe@PtRuFe, commercial PtRu/C and Pt/C catalysts recorded in 0.1 M $HClO_4$ solution containing 0.5 M methanol. As shown in the Fig. 4c and d, the onset potential of MOR on PtFe@PtRuFe catalyst is 0.416 V, which is 35 mV more negative than that of commercial PtRu/C (0.451 V) catalyst, ranking it among the better active MOR catalysts reported in the literature (Table S1). To gain further insights into the activity of different catalysts, the peak current at 0.75 V_{RHE} associated with MOR in the

forward scan was normalized with respect to both ECSA and the loading amount of metal Pt. As shown in Fig. 4e and Table S2, the PtFe@PtRuFe catalyst exhibit the highest specific activity of 1.30 mA.cm^{-2}, which is 1.57 and 8.6 times higher than the commercial PtRu/C (0.83 mA.cm^{-2}) and Pt/C (0.15 mA.cm^{-2}) catalysts, respectively. The mass activities of the PtFe@PtRuFe catalysts was found to be 0.69 mA.ug$_{Pt}^{-1}$, which is 1.68 and 6.3 times greater than the commercial PtRu/C (0.41 mA.ug$_{Pt}^{-1}$) and Pt/C (0.11 mA.ug$_{Pt}^{-1}$) catalysts, respectively. On the other hand, the current peak ratio of I_f (the forward peak current)/I_b (the backward peak current) for PtFe@PtRuFe is calculated to be 12.7, which is great higher than the PtRu/C (6) and Pt/C (0.72) catalyst. The higher I_f/I_b ratio implies that the methanol would be effectively oxidized during the forward potential scan and in the process of the backward potential scan could produce less CO_{ads} poisoning species, thereby the catalyst of PtFe@PtRuFe possess superior MOR activity and anti-CO poisoning ability [50,51]. The stability of Pt/C, PtRu/C and PtFe@PtRuFe towards MOR was evaluated under a constant potential of 0.75 V_{RHE} for 3000 s. The stability of Pt/C, PtRu/C and PtFe@PtRuFe towards MOR was evaluated under a constant potential of 0.75 V_{RHE} for 3000 s. The polarization currents decrease rapidly at the initial stage (Fig. 4f), which is
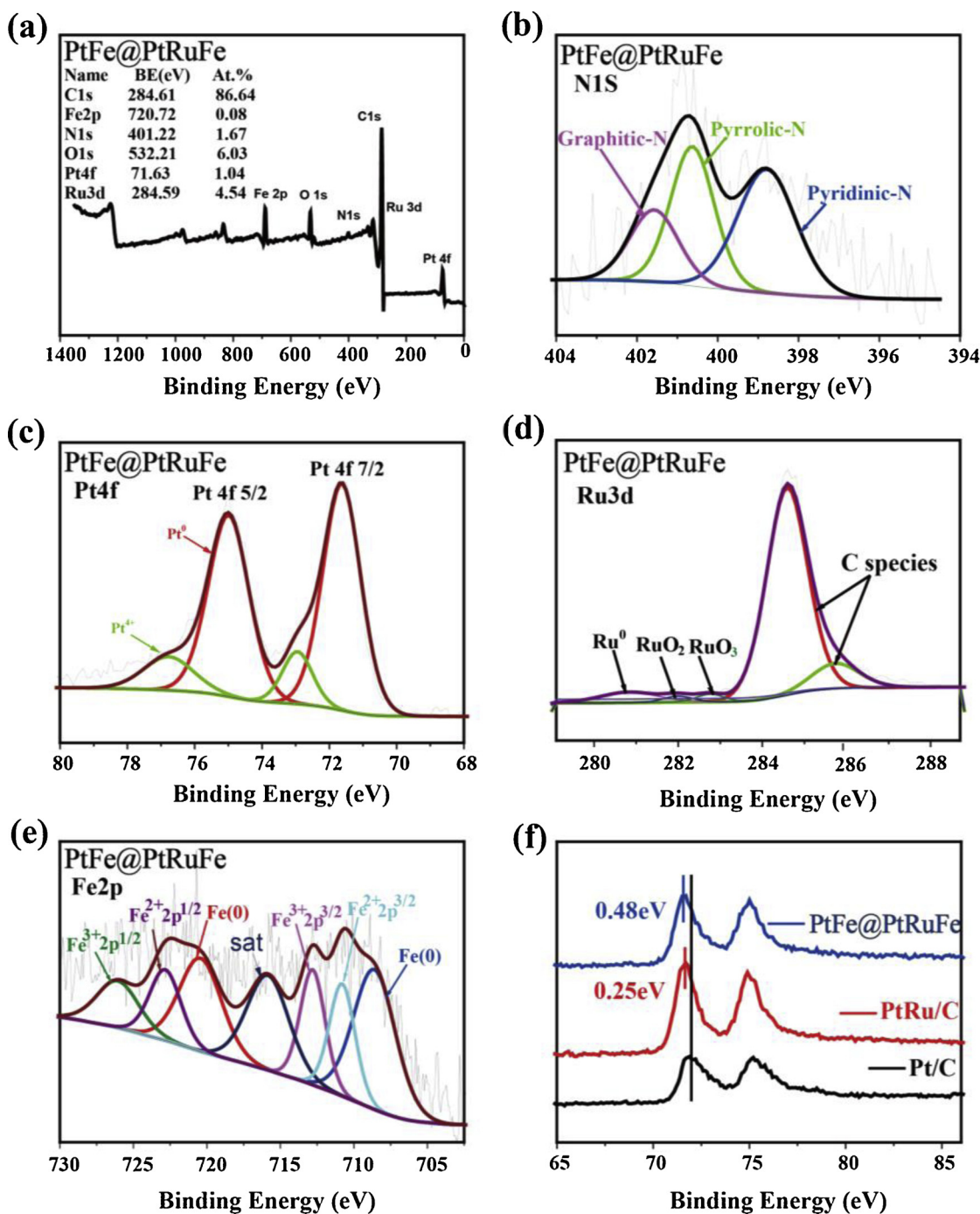
Fig. 3. (a) XPS survey of PtFe@PtRuFe. The deconvoluted peaks of N1S (b), Pt 4f (c), Ru 3d (d) and Fe 2p (e) spectra of PtFe@PtRuFe. (f) Comparison of Pt 4f XPS spectra for Pt/C, PtRu/C and PtFe@PtRuFe catalysts.

due to the formation of intermediate species during MOR [52]. However, the anodic current density of the PtFe@PtRuFe is higher than the PtRu/C and Pt/C catalysts during the entire time range, indicative of high electrocatalytic stability of the PtFe@PtRuFe in comparison with the PtRu/C and Pt/C catalysts. As shown in Figure. S9, the PtFe@ PtRuFe NPs are still homogeneously dispersed on carbon support after a constant potential of $0.75\,V_{RHE}$. These results again confirm the better anti-CO poisoning ability and improved electrocatalytic performance of the prepared PtFe@PtRuFe in MORs. The superior stability and the highest catalytic activity for MOR can be attributed to the unique core-shell nanostructure, in which the dissolution of the Ru and Fe atoms of NPs in an acidic condition and the formation of intermediate species might be effectively avoided [53–56].

4. Conclusion

In summary, we have successfully fabricated a well-defined PtFe@ PtRuFe core-shell nanostructure, composed of an ordered PtFe intermetallic core with a 3–5 atomic-layers-thick PtRuFe shell. The as-prepared PtFe@PtRuFe NPs exhibits improved electrocatalytic activity and durability for MOR as compared with commercial PtRu/C and Pt/C catalysts. The CO anodic oxidation on the PtFe@PtRuFe catalyst surface (0.39 V) starts much earlier than on the commercial PtRu/C (0.43 V) and Pt/C (0.83 V) catalysts, and the PtFe@PtRuFe exhibits the highest specific activity of $1.30\,mA.cm^{-2}$, which is 1.57 and 8.6 times higher than those of the PtRu/C ($0.83\,mA.cm^{-2}$) and Pt/C ($0.15\,mA.cm^{-2}$), respectively. The enhanced MOR activity and anti-CO poisoning ability
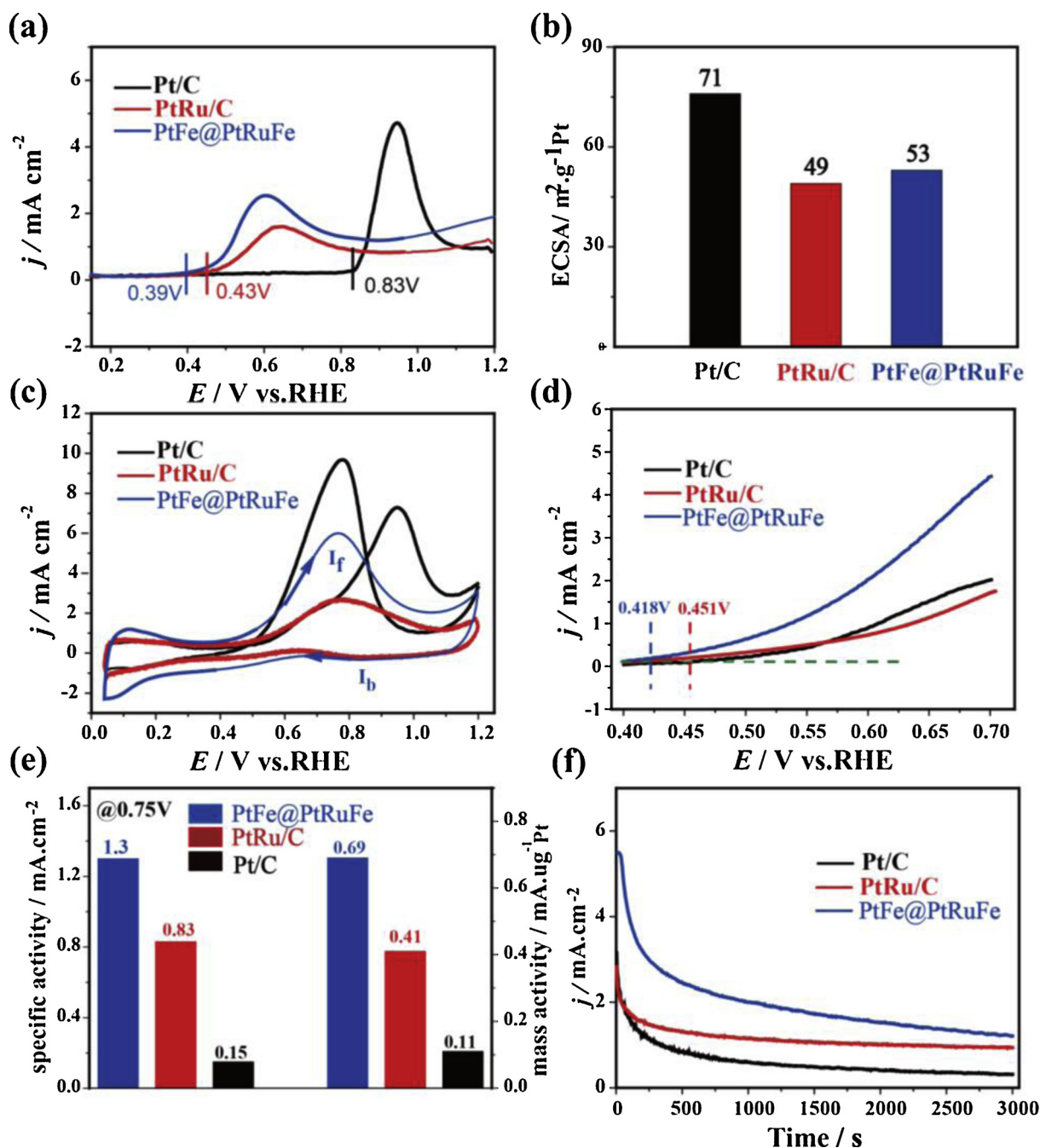
Fig. 4. (a) CO stripping voltammograms of Pt/C, PtRu/C, PtFe@PtRuFe catalysts in 0.1 M HClO$_4$ at a scan rate of 10 mV/s, and the corresponding ECSA (b). Cyclic voltammetry curves of Pt/C, PtRu/C, PtFe@PtRuFe catalysts in N$_2$-saturated 0.1 M HClO$_4$ solution containing 0.5 M methanol at a scan rate of 50 mV/s (c) and 10 mV/s (d) between 0.40V-0.75 V (e) The mass activity and specific activity of Pt/C, PtRu/C and PtFe@PtRuFe catalysts. (f) Chronoamperometry curves of Pt/C, PtRu/C and PtFe@PtRuFe catalysts in N$_2$-saturated 0.1 M HClO$_4$ solution containing 0.5 M methanol at 0.75 V.

of the PtFe@PtRuFe catalyst is ascribed to their well-defined core-shell structured and their favorable composition. This novel core-shell structured nanocatalyst provide a new direction to reduce the usage of noble metal, precisely adjusting the surface composition and atomic arrangement, enhance the activity and stability of multi-metallic alloy nanocatalyst.

Appendix A. Supplementary data

Supplementary material related to this article can be found, in the online version, at doi:https://doi.org/10.1016/j.apcatb.2019.04.023.

References

[1] A.R. de la Osa, A.B. Calcerrada, J.L. Valverde, E.A. Baranova, Ade. Lucas, Consuegra, Electrochemical reforming of alcohols on nanostructured platinumtin

catalyst electrodes, Appl. Catal. B Environ. 179 (2015) 276–284, https://doi.org/10.1016/j.apcatb.2015.05.026.

[2] Z. Hu, M. Wu, Z. Wei, S. Song, P.K. Shen, Pt-WC/C as a cathode electrocatalyst for hydrogen production by methanol electrolysis, J. Power Sources 166 (2007) 458–461, https://doi.org/10.1016/j.jpowsour.2007.01.083.

[3] C. Cui, L. Gan, M. Heggen, S. Rudi, P. Strasser, Compositional segregation in shaped Pt alloy nanoparticles and their structural behaviour during electrocatalysis, Nat. Mater. 12 (2013) 756–771, https://doi.org/10.1038/nmat3668.

[4] B. Qiao, A. Wang, X. Yang, L.F. Allard, Z. Jiang, Y. Cui, J. Liu, J. Li, T. Zhang, Single-atom catalysis of CO oxidation using Pt1/FeOx, Nat. Chem. 12 (2011) 634–641, https://doi.org/10.1038/nchem.1095.

[5] X.L. Tian, L.J. Wang, P.L. Deng, Y. Chen, B.Y. Xia, Research advances in un-supported Pt-based catalysts for electrochemical methanol oxidation, J. Energy Chem. 26 (2017) 1067–1076, https://doi.org/10.1016/j.jechem.2017.10.009.

[6] G. Long, X. Li, K. Wan, Z. Liang, J. Piao, P. Tsiakaras, Pt/CN-doped electrocatalysts: superior electrocatalytic activity for methanol oxidation reaction and mechanistic insight into interfacial enhancement, Appl. Catal. B Environ. 203 (2017) 541–548, https://doi.org/10.1016/j.apcatb.2018.04.017.

[7] H.K. Ju, S. Giddey, S.P. Badwal, The role of nanosized SnO2 in Pt-based electro-catalysts for hydrogen production in methanol assisted water electrolysis, Electrochim. Acta 229 (2017) 39–47, https://doi.org/10.1016/j.electacta.2017.01.106.

[8] E.I. Santiago, G.A. Camara, E.A. Ticianelli, CO tolerance on PtMo/C electrocatalysts prepared by the formic acid method, Electrochim. Acta 48 (2003) 3527–3534, https://doi.org/10.1016/S0013-4686(03)00474-2.

[9] J. Gu, Y.W. Zhang, F.F. Tao, Shape control of bimetallic nanocatalysts through well-designed colloidal chemistry approaches, Chem. Soc. Rev. 41 (2012) 8050–8065, https://doi.org/10.1039/c2cs35184f.

[10] Z.H. Yang, X.X. Yu, Q. Zhang, Remarkably stable CO tolerance of a PtRu electro-catalyst stabilized by a nitrogen doped carbon layer, RSC Adv. 6 (2016) 114014–114018, https://doi.org/10.1039/c6ra24548j.

[11] L. Wang, Y. Yamauchi, Metallic nanocages: synthesis of bimetallic Pt-Pd hollow nanoparticles with dendritic shells by selective chemical etching, J. Am. Chem. Soc. 135 (2013) 16762–16765, https://doi.org/10.1021/ja407773x.

[12] L. Bu, S. Guo, X. Zhang, X. Shen, D. Su, G. Lu, X. Zhu, J. Yao, J. Guo, X. Huang, Surface engineering of hierarchical platinum-cobalt nanowires for efficient elec-trocatalysis, Nat. Commun. 7 (2016) 11850, https://doi.org/10.1038/ncomms11850.

[13] C. Zhu, S. Guo, S. Dong, PdM (M = Pt, Au) bimetallic alloy nanowires with en-hanced electrocatalytic activity for electro-oxidation of small molecules, Adv. Mater. 24 (2012) 2326–2331, https://doi.org/10.1002/adma.201104951.

[14] S. Song, Y. Wang, P. Tsiakaras, P.K. Shen, Direct alcohol fuel cells: a novel non-platinum and alcohol inert ORR electrocatalyst, Appl. Catal. B Environ. 78 (2008) 381–387, https://doi.org/10.1016/j.apcatb.2007.09.037.

[15] R. Sriphathoorat, K. Wang, S.P. Luo, M. Tang, H.Y. Du, X.W. Du, P.K. Shen, K. Luo, M.H. Du, Y. Du, X.W. Shen, P. Kang, Well-defined PtNiCo core–shell nanodendrites with enhanced catalytic performance for methanol oxidation, J. Mater. Chem. A 4 (2016) 18015–18021, https://doi.org/10.1039/c6ta07370k.

[16] G.F. Long, X.H. Li, K. Wan, Z.X. Liang, J.H. Piao, P. Tsiakaras, Pt/CN-doped elec-trocatalysts: superior electrocatalytic activity for methanol oxidation reaction and mechanistic insight into interfacial enhancement, Appl. Catal. B Environ. 203 (2017) 541–548, https://doi.org/10.1016/j.apcatb.2016.10.055.

[17] S. Guo, S. Zhang, X. Sun, S. Sun, Synthesis of ultrathin FePtPd nanowires and their use as catalysts for methanol oxidation reaction, J. Am. Chem. Soc. 133 (2011) 15354–15357, https://doi.org/10.1021/ja207308b.

[18] R. Jiang, D. Chu, Comparative studies of methanol crossover and cell performance for a DMFC, J. Electrochem. Soc. 151 (A69) (2004), https://doi.org/10.1149/1.1629093.

[19] S. Song, W. Zhou, Z. Liang, R. Cai, G. Sun, Q. Xin, et al., The effect of methanol and ethanol cross-over on the performance of PtRu/C-based anode DAFCs, Appl. Catal. B Environ. 55 (2005) 65–72, https://doi.org/10.1016/j.apcatb.2004.05.017.

[20] Jeon Min, Ku Lee, Ki Rak Daimon, Hideo Nakahara, Akemi Woo, Seong Ihl, Pt45Ru45M10/C (M = Fe, Co, and Ni) catalysts for methanol electro-oxidation, Catal. Today 13 (2008) 123–126, https://doi.org/10.1016/j.cattod.2007.12.011.

[21] H.H. Li, S. Zhao, M. Gong, C.H. Cui, D. He, H.W. Liang, L. Wu, S.H. Yu, Ultrathin PtPdTe nanowires as superior catalysts for methanol electrooxidation, Angew. Chem. Int. Ed. 52 (2013) 7472–7476, https://doi.org/10.1002/anie.201302090.

[22] J. Xie, Q.H. Zhang, L. Gu, S.W. Xu, L. Peng, J.D. Guo, Y. Yi, Y.F. Nan, C.W. Zhao, Y.Y. Ming, Z.G. Zou, Ruthenium–platinum core–shell nanocatalysts with sub-stantially enhanced activity and durability towards methanol oxidation, Nano Energy 21 (2016) 247–257, https://doi.org/10.1016/j.nanoen.2016.01.013.

[23] Y. Yao, J. Cai, Y.L. Zheng, Y.X. Chen, Preparation of surfactant-free Pt and PtRu nanoparticles with high activity for methanol oxidation, Chin. J. Chem. Phys. 27 (2014) 332–336, https://doi.org/10.1063/1674-0068/27/03/332-336.

[24] D.H. Lee, J.L. You, J.M. Woo, J.Y. Seo, Y.C. Park, J.S. Lee, H.N. Kim, J.H. Moon, S.B. Park, Influence of dehydrating agents on the oxidative carbonylation of me-thanol for dimethyl carbonate synthesis over a Cu/Y-zeolite catalyst, Chin. J. Chem. Eng. 26 (2018) 1598-1598, https://doi.org/1016/S1872-2067(18)63020-7.

[25] T. Take, K. Tsurutani, M. Umeda, Hydrogen production by methanol-water solution electrolysis, J. Power Sources 164 (2007) 9–16, https://doi.org/10.1016/j.jpowsour.2006.10.011.

[26] L. Guo, S.G. Chen, L. Li, Z.D. Wei, A CO-tolerant PtRu catalyst supported on thiol-functionalized carbon nanotubes for the methanol oxidation reaction, J. Power Sources 247 (2014) 360–364, https://doi.org/10.1016/j.jpowsour.2013.08.102.

[27] H. Igarashi, J.T. Fu, Y.M. Zhu, H. Uchida, M. Watanabe, CO Tolerance of Pt alloy electrocatalysts for polymer electrolyte fuel cells and the detoxification mechanism,

[28] Phys. Chem. Chem. Phys. 3 (2001) 306–314, https://doi.org/10.1039/B007768M.

[28] L. Chen, C. Bock, P. Mercier, H.J. MacDougall, B. Ren, Ordered alloy formation for Pt3Fe/C, PtFe/C and Pt5.75Fe5.75Cuy/CO2-reduction electro-catalysts, Electrochim. Acta 27 (2012) 212–224, https://doi.org/10.1016/j.electacta.2012.05.103.

[29] Y. Zhang, J.F. Zhang, Z.L. Chen, Y.W. Liu, M.M. Zhang, X.P. Han, C. Zhong, W. Hu, B. Deng, Y. Deng, One-step synthesis of the PdPt bimetallic nanodendrites with controllable composition for methanol oxidation reaction, Sci. China Mater. 61 (2019) 697–706, https://doi.org/10.1007/s40843.

[30] J.E. Leffler, The enthalpy-entropy relationship and its implications for organic chemistry, J. Org. Chem. 20 (1955) 1203–1231.

[31] F. Otto, Y. Yang, H. Bei, E.P. George, Relative effects of enthalpy and entropy on the phase stability of equiatomic high-entropy alloys, Acta Mater. 61 (2013) 2628–2638.

[32] C.ésar R. Chamorro, María E. Mondéjar, Roberto Ramos, JoséJ. Segovia, María C. Martín, Miguel A. Villamañán, World geothermal power production status: Energy, environmental and economic study of high enthalpy technologies, Energy 42 (2012) 10e18.

[33] S. Dannefaer, P. Mascher, D. Kerr, Monovacancy formation enthalpy in silicon, Phys. Rev. Lett. 56 (1986) 2095–2198.

[34] Vivienne J. Thorn, Jan C.A. Boeyens, Gloria J. McDougall, Robert D. Hancock, Origin of the high ligand field strength and macrocyclic enthalpy in complexes of nitrogen-donor macrocycles, J. Am. Chem. Soc. 106 (1984) 3198–3207.

[35] Y.C. Yan, J.S. Du, Kyle D. Gilroy, D.R. Yang, Y.N. Xia, H. Zhang, Intermetallic na-nocrystals: syntheses and catalytic applications, Adv. Mater. 29 (2017) 1605997.

[36] C.H. Cui, H.H. Li, X.J. Liu, M.R. Gao, S.H. Yu, Surface composition and lattice or-dering-controlled activity and durability of CuPt electrocatalysts for oxygen re-duction reaction, ACS Catal. 2 (2012) 916–924, https://doi.org/10.1021/cs300058c.

[37] X.Y. Lang, G.F. Han, B.B. Xiao, L. Gu, Z.Z. Yang, Z. Wen, Y.F. Zhu, M. Zhao, J.C. Li, Q. Jiang, Mesostructured intermetallic compounds of platinum and non-transition metals for enhanced electrocatalysis of oxygen reduction reaction, Adv. Funct. Mater. 25 (2015) 230–237, https://doi.org/10.1002/adfm.201401868.

[38] A. Pavlišič, P. Jovanovič, V. Šelih, M. Šala, M. Bele, G. Dražic, I. Arčon, S. Hočevar, A. Kokalj, N. Hodnik, M. Gaberšček, Atomically resolved dealloying of structurally ordered Pt nanoalloy as an oxygen reduction reaction electrocatalyst, ACS Catal. 6 (2016) 5530, https://doi.org/10.1021/acscatal.6b00557.

[39] J.H. Qiu, M. He, M.M. Jia, J.F. Yao, Metal organic frameworks for Bi- and multi-metallic catalyst and their applications, Prog Chem. 28 (2016) 1016–1028, https://doi.org/10.1063/1674-0068/27/03/332-336.

[40] M.E. Scofield, C. Koenigsmann, L. Wang, H.Q. Liu, S.S. Wong, Tailoring the com-position of ultrathin, ternary alloy PtRuFe nanowires for the methanol oxidation reaction and formic acid oxidation reaction, Energy Environ. Sci. 8 (2015) 350–363, https://doi.org/10.1039/c4ee02162b.

[41] H.J. Liu, M.L. Dou, F.L. Wang, J.J. Jing, J. Li, Ordered intermetallic PtFe@Pt core-shell nanoparticles supported on carbon nanotubes with superior activity and durability as oxygen reduction reaction electrocatalysts, RSC Adv. 5 (2015) 66471–66475, https://doi.org/10.1039/c5ra12291k.

[42] X. Cui, P. Xiao, J. Wang, M. Zhou, W. Long, G.Y. Yang, J. He, Z.W. Wang, Y.K. Yang, Y.H. Zhang, Z.Q. Li, Highly branched metal alloy networks with superior activities for the methanol oxidation reaction, Angew. Chem. Int. Ed. 56 (2017) 4488–4493, https://doi.org/10.1002/anie.201701149.

[43] L.Z. Fang, Jackson Gregory, S. Eichhorn, W. Bryan, Tuning the CO-tolerance of Pt-Fe bimetallic nanoparticle electrocatalysts through architectural control, Energy Environ. Sci. 4 (2011) 1900, https://doi.org/10.1016/j.jechem.2017.10.009.

[44] Q. Feng, S. Zhao, D. He, S. Tian, L. Gu, X. Wen, C. Chen, Q. Peng, D. Wang, Y. Li, Strain engineering to enhance the electrooxidation performance of atomic-layer Pt on intermetallic Pt3Ga, J. Am. Chem. Soc. 140 (2018) 2773–2776, https://doi.org/10.1021/jacs.7b13612.

[45] B.Y. Xia, H.B. Wu, X. Wang, X.W. Lou, One-pot synthesis of cubic PtCu3 nanocages with enhanced electrocatalytic activity for the methanol oxidation reaction, J. Am. Chem. Soc. 134 (2012) 13934–13937, https://doi.org/10.1021/ja3051662.

[46] Z. Cui, H. Chen, M. Zhao, D. Marshall, Y. Yu, H. Abruna, F.J. DiSalvo, Synthesis of structurally ordered Pt3Ti and Pt3V nanoparticles as methanol oxidation catalysts, J. Am. Chem. Soc. 136 (2014) 10206–10209, https://doi.org/10.1021/ja504573a.

[47] Lee Jin, Yeon Han, Sang Beom Kwak, Da Hee Kim, Min Cheol Lee, Seul Park, JinYoung Choi, In Ae Park, Hyun Suk Park, Kyung Won, Porous Cu-rich@Cu3Pt alloy catalyst with a low Pt loading for enhanced electrocatalytic reactions, J. Am. Chem. Soc. 135 (2013) 16762–16765, https://doi.org/10.1021/ja407773x.

[48] S.Y. Ma, H.H. Li, B.C. Hu, X. Cheng, Q.Q. Fu, S.H. Yu, Synthesis of low Pt-Based quaternary PtPdRuTe nanotubes with optimized incorporation of Pd for enhanced electrocatalytic activity, J. Am. Chem. Soc. 139 (2017) 5890–5895, https://doi.org/10.1021/jacs.7b01482.

[49] Z.Y. Pedireddy, Srikanth Lee, Hiang Kwee, Y.J. Liu, T.J. Weng, Weei Phang, Yee In, X.Y. Ling, Manipulating the d-Band electronic structure of platinum-functionalized nanoporous gold bowls: synergistic intermetallic interactions enhance catalysis, Chem. Mater. 28 (2016) 5080–5086, https://doi.org/10.1039/c6ra24548j.

[50] Q.M. Wang, S.G. Chen, F. Shi, K. Chen, Y. Wang, R. Wu, J. Li, Y. Zhang, W. Ding, Y. Li, L. Li, Z.D. Wei, Structural evolution of solid Pt nanoparticles to a hollow PtFe alloy with a Pt-Skin surface via space-confined pyrolysis and the nanoscale kir-kendall effect, Adv. Mater. 28 (2016) 10673–10678.

[51] H.G. Zhao, W.H. Qi, X.F. Zhou, H.F. Wu, Y.J. Li, Composition-controlled synthesis of platinum and palladium nanoalloys as highly active electrocatalysts for methanol oxidation, Chin. Catal. 39 (2018) 342–349 https://doi.org/10.1016/S1872-2067(18)63020-7.

[52] T. Iwasita, Electrocatalysis of methanol oxidation, Electrochim. Acta 47 (2002) 3663–3674.

[53] S.Q. Lu, H.M. Li, J.Y. Sun, Z.B. Zhuang, Promoting the methanol oxidation catalytic activity by introducing surface nickel on platinum nanoparticles, Nano Res. 11 (2018) 2058–2068, https://doi.org/10.1007/s12274.

[54] L. Feng, L. Li, S. Zhong, L.W. Zhang, Y.Li. Xu, H. Shu, L. Shen, Facile synthesis of Pt-Cu (Ni, Co)/GNs-CD and their enhanced electro-catalytic activity for methanol oxidation, J. Electrochem. Soc. 163 (2016) F913–F918, https://doi.org/10.1149/2.1211608jes.

[55] Y. Yang, L.M. Luo, D. Chen, H.M. Liu, R.H. Zhang, Z.X. Dai, X.W. Zhou, Synthesis and electrocatalytic properties of PtPd nanocatalysts supported on graphene for methanol oxidation, Acta Phys. Chim. Sin. 33 (2017) 1628–1634, https://doi.org/10.3866/PKU.WHXB201704242.

[56] X.Qi. Lu, W.L. Wang, Z.G. Deng, H.Y. Zhu, S.X. Wei, N.S. Pang, W.Y. Guo, Chi. M. Wu. Lawrence, Methanol oxidation on Ru (0001) for direct methanol fuel cells: analysis of the competitive reaction mechanism, RSC Adv. 6 (2016) 1729–1737, https://doi.org/10.1039/c5ra21793h.